Werk

Jahr: 1979
Kollektion: fid.geo
Signatur: 8 Z NAT 2148:46
Digitalisiert: Niedersächsische Staats- und Universitätsbibliothek Göttingen
Werk Id: PPN1015067948_0046
PURL: http://resolver.sub.uni-goettingen.de/purl?PPN1015067948_0046

LOG Id: LOG_0026
LOG Titel: Magnetic ULF-Waves in the vicinity of active auroal forms
LOG Typ: article

Übergeordnetes Werk

Werk Id: PPN1015067948
PURL: http://resolver.sub.uni-goettingen.de/purl?PPN1015067948
OPAC: http://opac.sub.uni-goettingen.de/DB=1/PPN?PPN=1015067948

Contact

Niedersächsische Staats- und Universitätsbibliothek Göttingen
Georg-August-Universität Göttingen
Platz der Göttinger Sieben 1
37073 Göttingen
Germany
Email: gdz@sub.uni-goettingen.de

J. Geophys. 46, 229–236, 1979

Journal of Geophysics

Magnetic ULF-Waves in the Vicinity of Active Auroral Forms

N. Klöcker and B. Theile

Institut für Geophysik und Meteorologie der Technischen Universität Braunschweig, Mendelssohnstraße 1A, D-3300 Braunschweig, Federal Republic of Germany

Abstract. Magnetic field variations in the frequency range one to 5 Hz were measured with a rocket-borne magnetometer over an auroral arc during a substrom event. There is evidence that these fluctuations were produced by magnetohydrodynamic waves generated by ion gyroresonance. The payload was launched on October 13, 1977, from Andenes/Norway around magnetic midnight.

Key words: ULF-waves – Magnetohydrodynamic waves – Gyroresonance.

1. Introduction

In the frequency range 0.2–5 Hz of the electromagnetic spectrum a multitude of phenomena is observed on and near earth, e.g., pearls in geomagnetic micropulsations, auroral flickering, and microbursts in particle precipitation. Electric ULF waves in this frequency band have been detected within and above the ionospheric F-layer (Kintner and Cahill, 1978; Petelski et al., 1978). Recently published observations by the team of S-300 experimenters (1979) of the GEOS satellite show evidence of simultaneous magnetic and electric field fluctuations in the ULF frequency domain. An appropriate approach to explain these waves in terms of magnetohydrodynamics is to identify them as being either ion cyclotron or fast magnetosonic waves. These wave modes are believed to play an important role in wave-particle interaction (Cornwall, 1965; Cornwall, 1966; Kennel and Petschek, 1966; Cornwall et al., 1970).

Measurements of the magnetic field of these waves are still rare. The reason is twofold: (1) The spin frequency of sounding rockets and satellites is very often in the range of ULF band. Thus the waves can only be detected after very accurate restitution of the spacecraft's attitude in an earth-fixed frame of reference. (2) Most magnetometers flown on sounding rockets and near-earth satellites are not well suited to measure waves in the ULF band, e.g., due to limited dynamical range and limited time and amplitude resolution.

0340-062X/79/0046/0229/$01.60

We will present data which were measured with a three-component fluxgate magnetometer aboard a sounding rocket payload within the German IMS sounding rocket campaign 'substorm-phenomena'. The payload was equipped with a gyro based attitude control system. After a short outline of our instrument we describe the observations and rocket trajectory. The measurements will be introduced by an amplitude-time diagramme. We will then deal with the analysis of the waveforms and finally discuss some theoretical aspects.

2. Instrumentation

A three-component fluxgate magnetometer (Förstersonde type) is used. Full details of the instrument and the test philosophy were published elsewhere (Theile and Lühr, 1976). The instrument consists of an orthogonal sensor triple, an analogue and a digital electronic. The analogue electronic drives the sensor and transforms the returning signal into a voltage proportional to the field strength in the direction of the respective sensor axis. The dynamic range of the instrument's analogue output is 120,000 nT, the noise level is about 0.1 nT. A 16 bit analog to digital converter (ADC) is used to transform the output voltage into a digital telemetry compatible word. The input voltage of the ADC may only correspond to $\pm 30{,}000\,nT$ for the radially measured field components and 0–60,000 nT for the longitudinal (i.e., parallel to the spin axis) field component. This instrumental configuration allows the measurement of magnetic fields with a resolution of about 1 nT. The instrument responds to frequencies up to 500 Hz. There are no phase shifts and linearity errors for signals below 15 Hz. This instrumental property facilitates the analysis of the ULF waves.

The sampling rate amounts to 800 samples per channel per second. This high data rate is needed to compute highly accurate angles for the transformation of the magnetic field data into an earth fixed coordinate system.

3. Observations

The payload was launched on October 13, 1977, at 21 : 26 : 00 UT by a Skylark 12 from Andoya Rocket Range/Norway. A magnetospheric substorm had started at about 20 : 25 UT and continued until about 23 : 30 UT. The magnetic north component of the range magnetometer fluctuated around $-300\,nT$ during the payload's flight (21 : 26 – 21 : 38 UT). The payload reached an apogee of 536 km and splashed down at 540 km ground range distance.

A faint homogeneous arc was observed north of the range prior to launch. The launch decision was based on increasing micropulsation activity and the brightening of the arc. The intensity of the 557.7 nm auroral emission intensified to more than 50 kR shortly after launch. An auroral break-up occured at 21 : 31 UT followed by a rapid northward expansion of the aurora. Micropulsation activity prevailed throughout the flight. However, the pulsation magnetometer was not sensitive in the pc 1 range. The wave phenomena which will be treated here occurred around 21 : 35 UT. At that time the payload traversed an

Table 1. Velocities with respect to local geomagnetic field and spin frequencies for four selected times

Time after launch (s)	$V_\perp$ (ms^{-1})	$V_\parallel$ (ms^{-1})	Spinfrequency (Hz)
534.9	525	1,282	3.0033
538.1	519	1,307	3.0012
545.1	504	1,365	2.9921
549.1	496	1,398	2.9838

intensity maximum of an active auroral arc. More than 20 kR were measured for the λ557.7 nm oxygen line.

The measurements discussed here were made at 450 km altitude. The payload's velocity components parallel and perpendicular with respect to the earth's magnetic field as well as the spin frequency are listed in Table 1 for four selected times. The decrease of the spin frequency coincides with an increase of the payload's coning angle. This change of attitude parameters is caused by energy dissipation by long flexible booms tipped with probes for the electric field measurement. An activation of the attitude control system was necessary every 60 s.

Figure 1 shows a section of the original magnetometer data after transformation into an earth fixed coordinate system and deduction of a reference magnetic field as a function of time. The indicated times are seconds after lift-off. B_x points towards the magnetic north, B_y indicates the eastern direction, whereas B_z is parallel to the measured undisturbed geomagnetic field, i.e., pointing downwards with an angle of about 12 degrees with respect to the vertical.

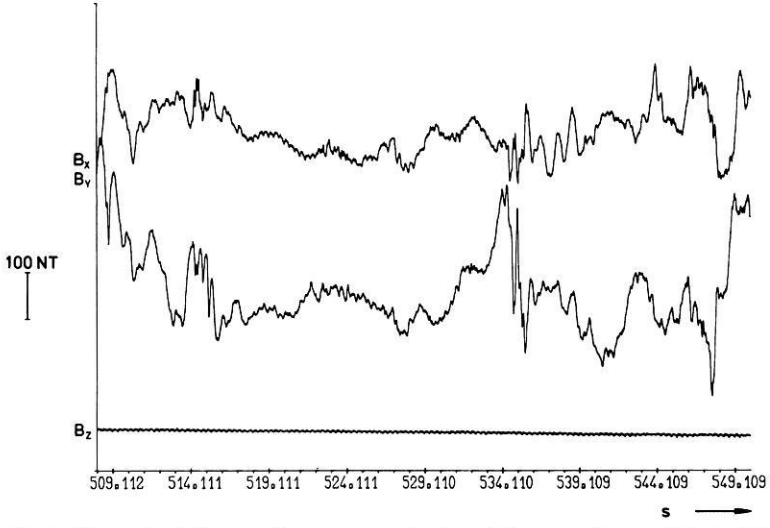

Fig. 1. Magnetic field variations measured aboard the sounding rocket payload (Substormphenomena F3A) on October 13, 1977. B_x-north, B_y-east, B_z-direction of earth's magnetic field vector. The abscissa gives seconds after launch which took place at 21:26:00 UT

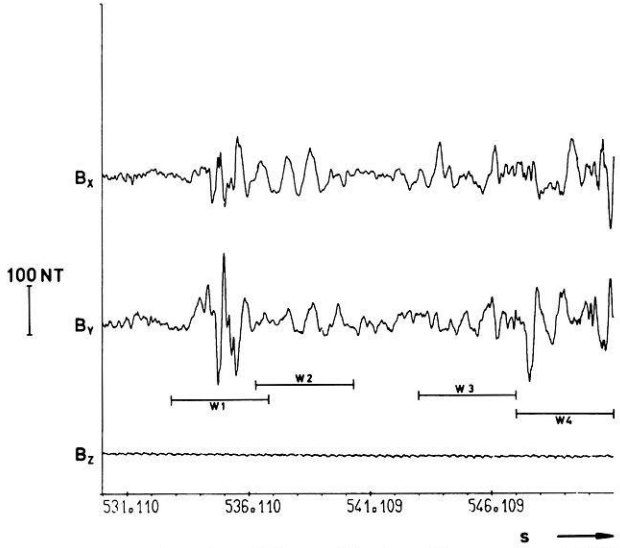

Fig. 2. Data section after high-pass filtering with cut-off at 0.65 Hz was applied. The windows $W1$–$W4$ mark those intervalls which were Fourier-transformed for spectral analysis

The transformation is carried out by a mere rotation of the sensor-based coordinate system. The reference directions for the transformation angles are established by the measured geomagnetic field and the direction of the payload's total angular momentum. The latter is computed using attitude data of the gyro based attitude control system. The payload's rotational motions are being represented by a set of time dependent analytical functions. These functions are coupled by gyroscopic laws. A new set of initial conditions must be determined after each activation of the attitude control system. Thus each interval between two attitude control system activations requires new parameters for the analytical description of the rotational motions. Consequently only magnetic field variations with periods below 60 s (i.e., the time interval between two attitude control system activations) can be analysed.

Field variations with different amplitudes and periods can be identified in B_x and B_y. Variations in B_z cannot be observed. The conclusion of this observational evidence is that the longitudinal (i.e., parallel to the earth's magnetic field) component of the field variation must be below $1\,nT$. With an order of magnitude of $100\,nT$ for the transverse component we deduce by statistical analysis that the angle of the field variation vector must be between 89.5 and 90.5 degrees with respect to the local geometric field. The fluctuations with longer periods ($T \sim 40$ s) seen in Fig. 1 may be of temporal or spatial nature. They will not be discussed here.

Further analysis and discussion will be dedicated to variations at frequencies of more than 1 Hz. Magnetic variations transverse to the main field may be due to either field-aligned currents or to magnetohydrodynamic waves. The current density of a field-aligned current sheet can be computed by using the first Maxwell equation. Assuming an east-west current sheet of infinite extent and a payload displacement towards north (x-direction), we find for the current

density $j=1/\mu_0 \cdot dB_y/dx$. The numerical evaluation results in a current density of $10^{-3}\,\mathrm{Am}^{-2}$, a value of unrealistic high magnitude. Thus we consider these variations as being due to waves.

The data are prepared for further analysis by being high pass filtered. The cut-off frequency is 0.65 Hz. The result is shown in Fig. 2. Some periodic structures can be identified.

4. Analysis

Further analysis will be carried out by Fourier transformation of selected time intervals. These intervals are marked in Fig. 2 by bars and are identified by the designations $W1$ through $W4$. The waves can be dissolved into two circularly polarized waves with opposite senses of rotation.
Considering only the transverse field components we write

$$B_x = B_{x_0} e^{i(\omega t + \phi_x)} \tag{1}$$

$$B_y = B_{y_0} e^{i(\omega t + \phi_y)} \tag{2}$$

The right hand polarization is then given by

$$B_R = \tfrac{1}{2}(B_x + iB_y) \tag{3}$$

and the left hand mode by

$$B_L = \tfrac{1}{2}(B_x^* + iB_y^*) \tag{4}$$

where the asterisk stands for the complex conjugate.

The windows $W1$ through $W4$ are bilaterally smoothed by a cosine function:

$$\omega(t) = \begin{cases} \dfrac{1}{2T}\left(1+\cos\dfrac{\pi}{(1-a)T}t\right) & aT \leqq |t| \leqq T \\ \dfrac{1}{T} & -aT < t < aT \end{cases} \tag{5}$$

The main lobe of the transformed window $W(t)$ has an effective width of 0.4 Hz ($T=2$ s, $a=0.4$). The first side lobe shows a maximum transfer ratio of 0.3 at 0.48 Hz.

The instrument's noise is $1\,nT$. The spectral estimates were optimized by varying the window length. Spectral peaks protruding by more than $2\,nT$ must be considered to be real signals. However, there is one exemption in the left-hand polarized spectrum of Fig. 4: the peak at 3 Hz is caused by a not completely corrected misalignment of a sensor axis.

Figure 3 shows the spectra of the right-hand (r-mode) and the left-hand (l-mode) polarized waves belonging to window $W1$. The r-mode spectrum is characterized by two maxima at 0.5 and 1.3 Hz which do not appear in the l-mode spectrum. At frequencies higher than 2 Hz the l- and r-mode spectra are almost the same which means that the wave is linearly polarized.

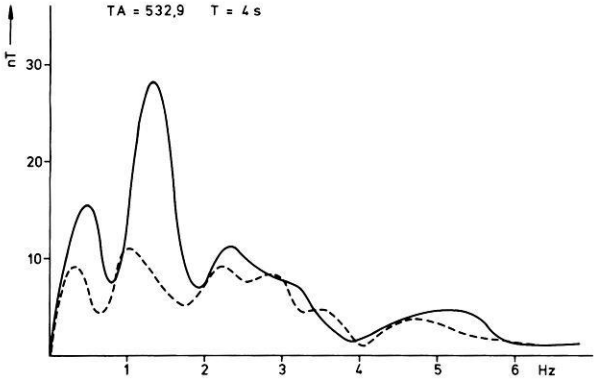

Fig. 3. Spectrum of window $W1$ for the right-hand polarized (*solid line*) and the left-hand polarized (*dashed line*) wave. The statistical significance is discussed in Sect. 4

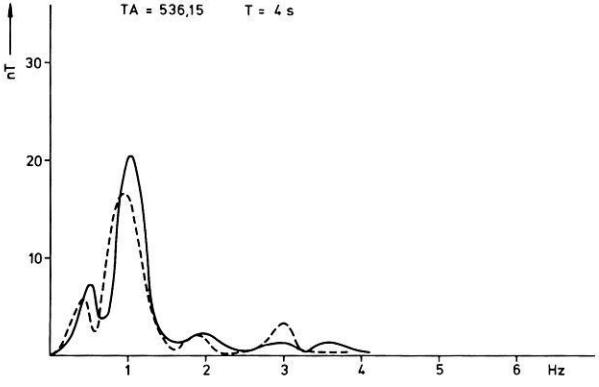

Fig. 4. Spectrum of window $W2$

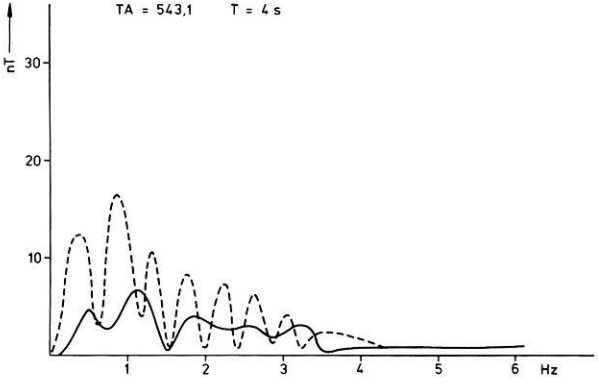

Fig. 5. Spectrum of windows $W3$

It should be mentioned, that a field-aligned proton flux at 65 keV was observed between 534 and 536 s after launch (W. Stüdemann, private communication), that is within this window. The continuation is shown by the second window $W2$ in Fig. 4. The wave becomes nearly linearly polarized and almost monochromatic at 1 Hz.

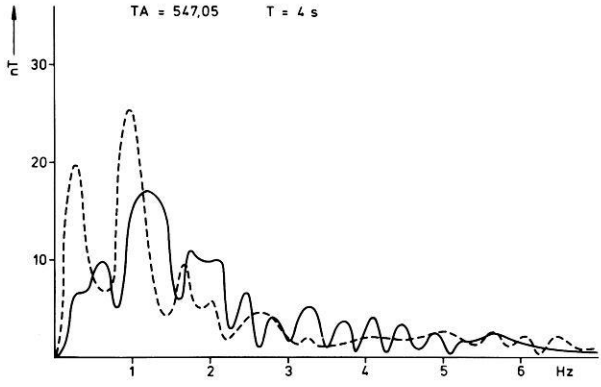

Fig. 6. Spectrum of window $W4$

The spectra of windows $W3$ and $W4$ are shown in Figs. 5 and 6. The l-mode-spectrum of Fig. 5 is characterised by peaks at integer multiples of 0.437 Hz. The r-mode-spectrum is not well defined. Figure 6 shows multiples of 0.4 Hz in the r-mode-spectrum. These multiples can be clearly identified above 2 Hz.

A common feature of all spectra is a shift of corresponding maxima in the l- and r-mode-spectra. The spectrum of $W2$ (Fig. 4) shows a shift of 0.1 Hz with all three peaks. The right-mode maximum is always shifted towards the higher frequency. This phenomena can be explained by a 0.05 Hz clockwise rotation of the ambient plasma with respect to an earth fixed coordinate system.

5. Discussion

The plasma of the inner magnetosphere is characterized by a very low ratio of the thermal velocity to the Alfén velocity. Thus, with $v_{th}^2/v_A^2=\beta\ll 1$ we find two wave modes being candidates to explain our observations: The anisotropic Alfvén mode for ions (left-hand polarization) and the fast magnetosonic mode (right-hand polarization). The instable growth mechanism of these modes has been investigated by Cornwall (1965) as well as by Kennel and Petschek (1966).

In order to explain the waves measured between 532 and 540 s after launch, we assume a cause and effect relationship between the above quoted field-aligned ion beam at 536 s and the wave phenomena.

The observations within windows $W1$ and $W2$ together with the field-aligned protons are consistent with Kennel and Petschek's (1966) conditions for the magnetosonic mode near ion gyroresonance. The resonant frequency of a gyroresonance interaction is determined by the ratio of the parallel energy (E_R) to the magnetic energy (E_C) per particle. This ratio is determined by

$$\frac{E_R}{E_C}=\left(\frac{\omega_i}{\omega}\right)^2\left(1+\frac{\omega}{\omega_i}\right)^3 \tag{6}$$

ω_i – Ion gyrofrequency
ω – Wave frequency

$E_R = \frac{1}{2} m_i v_R^2$ parallel energy
$E_C = B^2/2\mu_0 N$ magnetic energy
m_i – Ion mass
v_R – Resonant velocity
B – Magnitude of magnetic field
N – Number density.

According to Kennel and Petschek (1966) the waves can only be generated near the equator, because E_C grows fast away from the equator. We find for $L \gtrsim 7$ where the measurements were taken $\omega_i = 9\,\mathrm{rad \cdot s^{-1}}$ and $E_C \approx 10\,\mathrm{keV}$. From our measurements we get $\omega = 2\pi f = 8\,\mathrm{rad\,s^{-1}}$. Thus, $E_R/E_C = 8$, which is consistent with the particle observations (Stüdemann, internal report, 1979). Protons are the only candidates for this resonance interaction as for heavier ions $\omega_i > \omega$ would be no longer valid.

We do not have an adequate explanation for a possible relationship of the spectra shown in Figs. 5 and 6. Higher harmonics can be excited, if the wave vector is inclined against the magnetic field (Stix, 1962). However, these waves ought to be elliptically polarized, which is not observed in our case.

Acknowledgements. We thank Professor Dr. W. Kertz, Direktor des Institutes für Geophysik und Meteorologie der TU Braunschweig, for many fruitful discussions and steady support of the project. H. Lühr performed most of the hardware tests. Dr. Wilhelm, Max-Planck-Institut für Aeronomie in Lindau, acted as project scientist. The project was financed by Bundesministerium für Forschung und Technologie and managed by Deutsche Forschungs- und Versuchsanstalt für Luft- und Raumfahrt.

References

Cornwall, J.M.: Cyclotron instabilities and electromagnetic emission in the ultra low frequency and very low frequency ranges. J. Geophys. Res. **70**, 61–69, 1965

Cornwall, J.M.: Micropulsations and the outer radiation zone. J. Geophys. Res. **71**, 2185–2199, 1966

Cornwall, J.M., Coroniti, F.V., Thorne, R.M.: Turbulent loss of ring current protons. J. Geophys. Res. **75**, 4699–4709, 1970

Kennel, C.F., Petschek, H.E.: Limit on stably trapped particle fluxes. J. Geophys. Res. **71**, 1–28, 1966

Kintner, P.M., Cahill, L.J.: Electric field oscillations measured near an auroral arc. Planet. Space Sci. **26**, 555–558, 1978

Petelski, E.F., Fahleson, U., Shawhan, S.D.: Models for quasiperiodic electric fields and associated electron precipitation in the auroral zone. J. Geophys. Res. **83**, 2489–2498, 1978

S-300 Experimenters: Measurements of electric and magnetic wave fields and of cold plasma parameters on-bord GEOS-1. Preliminary results. Planet. Space Sci. **27**, 317–339, 1979

Stix, T.H.: The theory of plasma waves. New York, San Francisco, Toronto, London: McGraw-Hill Book Company, Inc. 1962

Theile, B., Lühr, H.: Magnetfeldmessungen an Bord von Höhenforschungsraketen. Raumfahrtforschung **20**, 301–305, 1976

Received May 29, 1979; Revised Version September 19, 1979; Accepted September 22, 1979